BIOCHEMISTRY
including biophysical chemistry & molecular biology

Article

pubs.acs.org/biochemistry

Structural Insight into MtmC, a Bifunctional Ketoreductase-Methyltransferase Involved in the Assembly of the Mithramycin Trisaccharide Chain

Jhong-Min Chen, Caixia Hou, Guojun Wang, Oleg V. Tsodikov,* and Jürgen Rohr*

Department of Pharmaceutical Sciences, College of Pharmacy, University of Kentucky, 789 South Limestone Street, Lexington, Kentucky 40536-0596, United States

Supporting Information

ABSTRACT: More and more post-PKS tailoring enzymes are recognized as being multifunctional and codependent on other tailoring enzymes. One of the recently discovered intriguing examples is MtmC, a bifunctional TDP-4-keto-D-olivose ketoreductase-methyltransferase, which—in codependence with glycosyltransferase MtmGIV—is a key contributor to the biosynthesis of the critical trisaccharide chain of the antitumor antibiotic mithramycin (MTM), produced by *Streptomyces argillaceus*. We report crystal structures of three binary complexes of MtmC with its methylation cosubstrate SAM, its coproduct SAH, and a nucleotide TDP as well as crystal structures of two ternary complexes, MtmC-SAH-TDP-4-keto-D-olivose and MtmC-SAM-TDP, in the range of 2.2−2.7 Å resolution. The structures reveal general and sugar-specific recognition and catalytic structural features of MtmC. Depending on the catalytic function that is conducted by MtmC, it must bind either NADPH or SAM in the same cofactor binding pocket. A tyrosine residue (Tyr79) appears as a lid covering the sugar moiety of the substrate during the methyl transfer reaction. This residue swings out of the active site by ∼180° in the absence of the substrate. This unique conformational change likely serves to release the methylated product and, possibly, to open the active site for binding the bulkier cosubstrate NADPH prior to the reduction reaction.

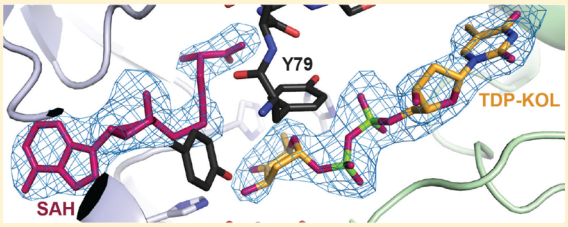

Mithramycin **1** [MTM (Figure 1)] is a member of the aureolic acid family of antitumor antibiotics that also includes the chromomycins, olivomycin, durhamycin A, UCH9, and chromocyclomycin.[1−4] Aureolic acids act on Gram-positive bacteria and inhibit growth and multiplication of several cancer cell lines through disregulation of transcription, by interacting in a Mg^{2+}-dependent manner with the minor groove of GC-rich regions of DNA.[5,6] Durhamycin A is also an inhibitor of HIV Tat transactivation.[4] Additionally, chromomycin and MTM are strong inducers of erythroid differentiation in K562 cells and potent inhibitors of neuronal apoptosis, making these compounds candidates for therapeutics of hematological diseases and neurological disorders, respectively.[7] MTM was recently discovered as the only drug of 50000 screened compounds to potently antagonize the abnormal oncogenic transcription factor EWS-FLI1 in Ewing sarcoma, a poorly treatable bone and soft tissue cancer that affects mostly children and young adults.[8] MTM is currently in clinical trials for the treatment of this devastating cancer (National Cancer Institute, clinical trial NCT01610570). MTM was also identified as a potent downregulator of ABCG2 efflux pumps,[9] whose overexpression is responsible for resistance to lung cancer chemotherapeutics. MTM recently entered clinical trials for the treatment of cancers of the respiratory tract, including esophageal and lung cancers (National Cancer Institute, clinical trial NCT01624090).

MTM and all other aureolic acid compounds (except chromocylomycin) contain a tricyclic chromophore with two oligosaccharide chains attached via *O*-glycosidic bonds at positions C-2 and C-6 of the aglycone, respectively, as well as two aliphatic side chains at positions C-3 and C-7, respectively (Figure 1). The aglycone is formed by a type 2 polyketide synthase (PKS) from one acetyl-CoA and nine malonyl-CoA units.[10−13] In each aureolic acid compound, except durhamycin A and UCH9, the oligosaccharides at positions C-2 and C-6 are di- and trisaccharide chains, respectively, and they contain unique deoxyhexose sugars. The trisaccharide chain of MTM is a key structural part that appears to be evolutionarily optimized for binding DNA in a minor groove of GC-rich regions. This chain contains a D-olivose (sugar C), a D-oliose (sugar D), and a D-mycarose (sugar E). Although this chain contains three sugar units, its biosynthesis requires only two glycosyltransferases, namely, MtmGIV and MtmGIII. MtmGIV initiates the glycosylation cascade by transferring a D-olivose moiety to the aglycone precursor premithramycinone and finishes the trisaccharide chain by transferring a D-mycarose unit (Figure 2).[14] MtmGIII acts by transferring the middle sugar, D-oliose.[15,16] Both of the MtmGIV-catalyzed steps are supported by MtmC, which, in situ, generates either TDP-D-olivose by

Received: November 26, 2014
Revised: January 14, 2015
Published: January 14, 2015

DOI: 10.1021/bi501462g
Biochemistry 2015, 54, 2481−2489

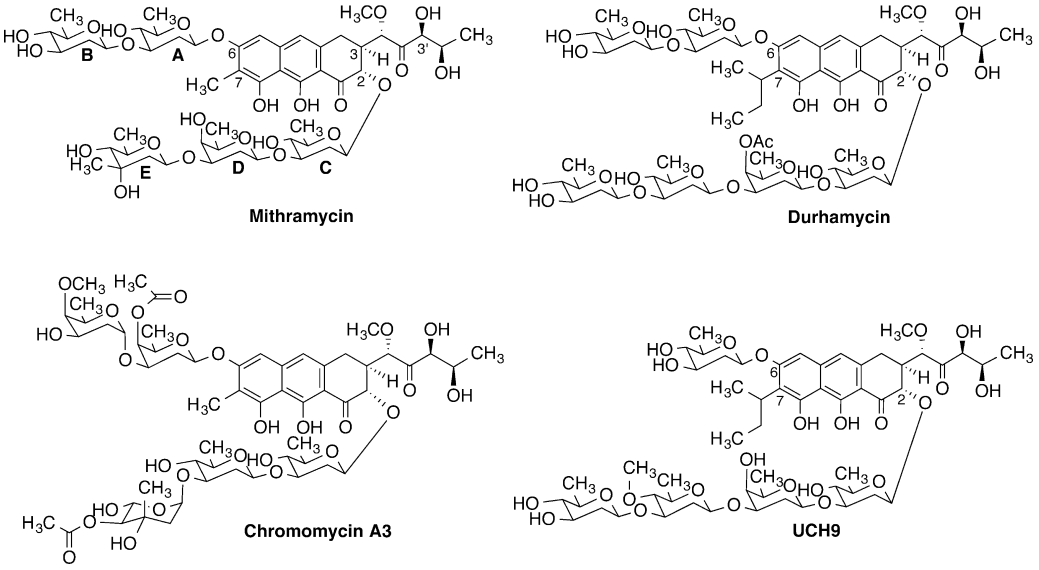

Figure 1. Chemical structures of MTM and other representative aureolic acid drugs.

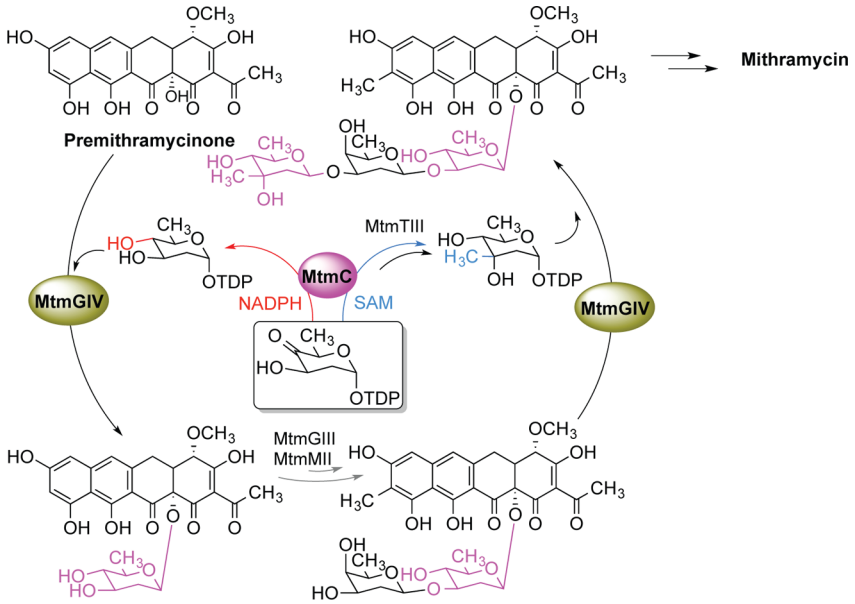

Figure 2. Biosynthetic route for generation of the trisaccharide chain of MTM, highlighting the central role of MtmC and MtmGIV in the sugar elaboration of the chain assembly.

reduction or TDP-D-4-keto-mycarose by methylation from the same precursor, TDP-4-keto-D-olivose (TDP-KOL).[17] Furthermore, MtmTIII is required for the reduction of 4-keto-D-mycarose to D-mycarose, either prior or immediately after the glycosyl transfer step.[14] Therefore, activities of MtmC, MtmGIV, and MtmTIII need to be coordinated. How these enzymes cooperate remains one of the most intriguing mysteries of the MTM biosynthetic pathway. Here we present the first piece of the puzzle of the multifaceted biosynthesis of MTM's trisaccharide chain, the crystal structure of the bifunctional ketoreductase-methyltransferase MtmC.

MATERIALS AND METHODS

Protein Expression and Purification and Site-Directed Mutagenesis of MtmC. The original annotated sequence of the *mtmC* gene from *Streptomyces argillaceus* contained inaccuracies; the corrected sequence was deposited into GenBank as entries GUSub26197 and GUSub26196 for the amino acid residue and nucleotide sequences, respectively. MtmC protein was expressed following a previously reported protocol.[17] The fractions containing MtmC were pooled and dialyzed against 20 mM Tris (pH 7.5), 100 mM M NaCl, 2 mM β-mercaptoethanol, and 10% glycerol. For biochemical assays, the enzyme was concentrated to 14 mg/mL, flash-frozen, and stored at −80 °C. For crystallization, the purified protein was further passed through a size-exclusion Sephacryl S-200 column (GE Healthcare) equilibrated in 40 mM Tris-HCl (pH 8.0) (pH adjusted at room temperature), 0.1 M NaCl, and 2 mM β-mercaptoethanol, and the fractions containing the protein were pooled and concentrated using an Amicon Ultra-15 centrifugal filter device (Millipore) to 12 mg/mL.

MtmC Tyr79Phe and MtmC Tyr79Ala mutants were generated by site-directed mutagenesis with the QuikChange kit (Stratagene), following the manufacturer's protocol.

DOI: 10.1021/bi501462g
Biochemistry 2015, 54, 2481−2489

Table 1. X-ray Diffraction Data Collection and Structural Refinement Statistics

	MtmC-SAH-TDP-KOL	MtmC-SAM-TDP	MtmC-SAM	MtmC-SAH	MtmC-TDP
			Data Collection[a]		
space group	$I4_122$	$I4_122$	$I4_122$	$I4_122$	$I4_122$
no. of monomers per asymmetric unit	1	1	1	1	1
unit cell dimensions					
a, *b*, *c* (Å)	135.4, 135.4, 127.3	134.7, 134.7, 127.8	134.8, 134.8, 129.7	134.2, 134.2, 130.0	134.2, 134.2, 132.3
α, β, γ (deg)	90, 90, 90	90, 90, 90	90, 90, 90	90, 90, 90	90, 90, 90
resolution (Å)	50−2.35 (2.39−2.35)	50−2.3 (2.34−2.30)	50−2.2 (2.24−2.20)	50−2.2 (2.24−2.20)	50−2.7 (2.8−2.7)
I/σ	28.2 (2.5)	40.3 (4.7)	39.9 (3.2)	41.8 (3.7)	25.2 (3.3)
completeness (%)	95.7 (98.9)	99.5 (100)	100 (100)	99.0 (100)	100 (100)
redundancy	6.6 (6.5)	9.8 (10)	8.1 (8.2)	9.6 (9.8)	9.7 (10.0)
R_{merge}	0.075 (0.61)	0.077 (0.499)	0.064 (0.625)	0.087 (0.627)	0.129 (0.676)
no. of unique reflections	21204	24771	28993	28774	16056
			Structural Refinement		
resolution (Å)	40−2.35	40−2.3	40−2.2	40−2.2	40−2.7
R (%)	20.6	21.2	21.4	20.3	20.9
R_{free} (%)	23.1	23.8	25.7	24.1	24.8
rmsd from ideal					
bond lengths (Å)	0.005	0.005	0.006	0.006	0.005
bond angles (deg)	1.01	1.08	1.13	1.1	0.97
Ramachadran plot[b] (% residues by region)					
most allowed	98.1	97.1	92.2	97.8	90.5
additional allowed	1.9	2.9	7.3	2.2	8.7
generously allowed	0	0	0.6	0	0.3
disallowed	0	0	0	0	0.6 (two residues)[c]

[a]Values in parentheses refer to data for the highest-resolution shell. [b]PROCHECK statistics.[33] [c]The outliers (His178 and Ser82), which are both in or near the active site, fall in the immediate vicinity of the allowed regions of the Ramachandran plot, within the uncertainty of the modest resolution of the MtmC-TDP structure. His178 faces the active site pocket, and its conformation may be somewhat strained by binding of the unnatural TDP ligand; Ser82 is in the sensor loop and is somewhat disordered in this complex.

Incorporation of the desired mutation into each plasmid was confirmed by DNA sequencing at the University of Kentucky DNA Sequencing Core. Mutant proteins were expressed and purified like the wild-type enzyme.

Crystallization, Data Collection, and Crystal Structure Determination. The initial crystallization condition was found by a sparse incomplete factorial screen (Hampton Research Crystal Screen), by vapor diffusion in hanging drops at 21 °C. Under the optimized conditions, the drops contained 1 μL of MtmC with 1 mM ligand (SAM, SAH, TDP, TDP-4-keto-D-olivose, or their mixtures, as specified) and 1 μL of the reservoir solution [0.1 M MES (pH 5.5), 0.2 M ammonium acetate, and 16% PEG 4000]. The crystals were gradually transferred into the cryoprotectant buffer [0.1 M MES (pH 5.5), 0.2 M ammonium acetate, 16% PEG 4000, and 20% glycerol] and rapidly frozen in liquid nitrogen.

X-ray diffraction data were collected at 100 K at beamlines 21ID-G (for MtmC-SAM-TDP crystals) and 22ID (for the other crystals) of the Advanced Photon Source at the Argonne National Laboratory (Argonne, IL). The data were processed with HKL2000.[18] The structure of the MtmC-SAM-TDP complex was determined by molecular replacement with MOLREP[19] with the structure of methyltransferase TcaB9 [Protein Data Bank (PDB) entry 4E2X][20] as a search model. The structure was then iteratively rebuilt and refined with COOT[21] and REFMAC.[22] The ligands in this and other structures were modeled without uncertainty into strong omit $F_o - F_c$ electron density. The structure of the MtmC-SAM-TDP complex served as a starting point for rebuilding and refinement of all other structures of MtmC. The data collection and refinement statistics are listed in Table 1. Crystal structures listed in Table 1 were deposited in the PDB as entries 4RV9 (complex with SAH), 4RVD (complex with SAM), 4RVF (complex with TDP), 4RVG (complex with SAM and TDP), and 4RVH (complex with SAH and TDP-4-keto-D-olivose).

Methyltranferase Activity Assays. The product of the 3-methylation reaction by wild-type MtmC, TDP-4-keto-D-mycarose, could not be observed likely because the axial 3-OH group generated concomitantly with 3-methylation attacked the proximal phosphate to cleave the phosphodiester bond of TDP, resulting in the loss of UV absorbance.[17] For this reason, we monitored formation of the coproduct SAH. Kinetic assays were conducted for the wild-type and mutant MtmC (Tyr79Phe and Tyr79Ala) by discontinuous HPLC (Waters 600 system, consisting of a controller, a Waters 996 photodiode array detector, and a Delta 600 pump). A 100 μL reaction mixture contained 25 mM Hepes (pH 7.5), 50 mM NaCl, 1 mM EDTA, 90 μM TDP-KOL, 2 mM SAM, and 5 μM MtmC. The reactions were initiated by the addition of enzyme and the mixtures incubated at 22 °C, to minimize the nonenzymatic degradation of SAM; 50 μL aliquots were quenched at 60 and 300 min (in the range where the SAH concentration increased linearly over time) with 5 μL of 1.5 g/mL trichloroacetic acid [final concentration of 13.6% (w/v)] and then incubated on ice for 10 min. After centrifugation at 13000 rpm for 3 min, 50 μL of the supernatant was passed through a Phenomenex Kinetex 5 μm EVO C18 100 Å column (250 mm × 4.6 mm) and eluted isocratically in 10 mM ammonium formate with 5% methanol (pH 3.0) at a rate of 0.8 mL/min. The area under the chromatogram absorbance peak at 260 nm corresponding to

DOI: 10.1021/bi501462g
Biochemistry 2015, 54, 2481−2489

Table 2. MtmC and Its Homologues

protein	bacterium	sugar product	pathway product	ref
MtmC	*S. argillaceus*	D-mycarose/D-olivose	mithramycin	this study and 17
SnoG[a]	*Streptomyces nogalater*	nogalose	nogalamycin	34
CloU	*Streptomyces roseochromogenes* var. *oscitans* DS12.976	5,5-*gem*-dimethyl deoxysugar (GDD)	clorobiocin	25
CouU	*Streptomyces rishiriensis*	GDD	coumermycin A_1	26, 27
NovU	*Streptomyces spheroides* (*niveus*)	GDD noviose	novobiocin	28
ORF14/SmtA	*Amycolatopsis orientalis*	vancosamine	chloroeremomycin/ vancomycin	35
TcaB9	*M. chalcea*	D-tetronitrose	tetrocarcin A	20, 24
TiaS2	*Dactylosporangium aurantiacum* subsp. *hamdegenensis* NRRL 18085	modified D-rhamnose	tiacumicin B	29
EryBIII	*Saccharopolyspora erythraea*	modified L-mycarose	erythromycin A	30
TylCIII	*Streptomyces fradiae*	L-mycarose	tylosin	31
AviG1	*Streptomyces viridochromogenes* Tü57	L-mycarose	avilamycin	32

[a]The homologues are presented in the order of their level of sequence similarity to MtmC, from the most to the least similar homologues.

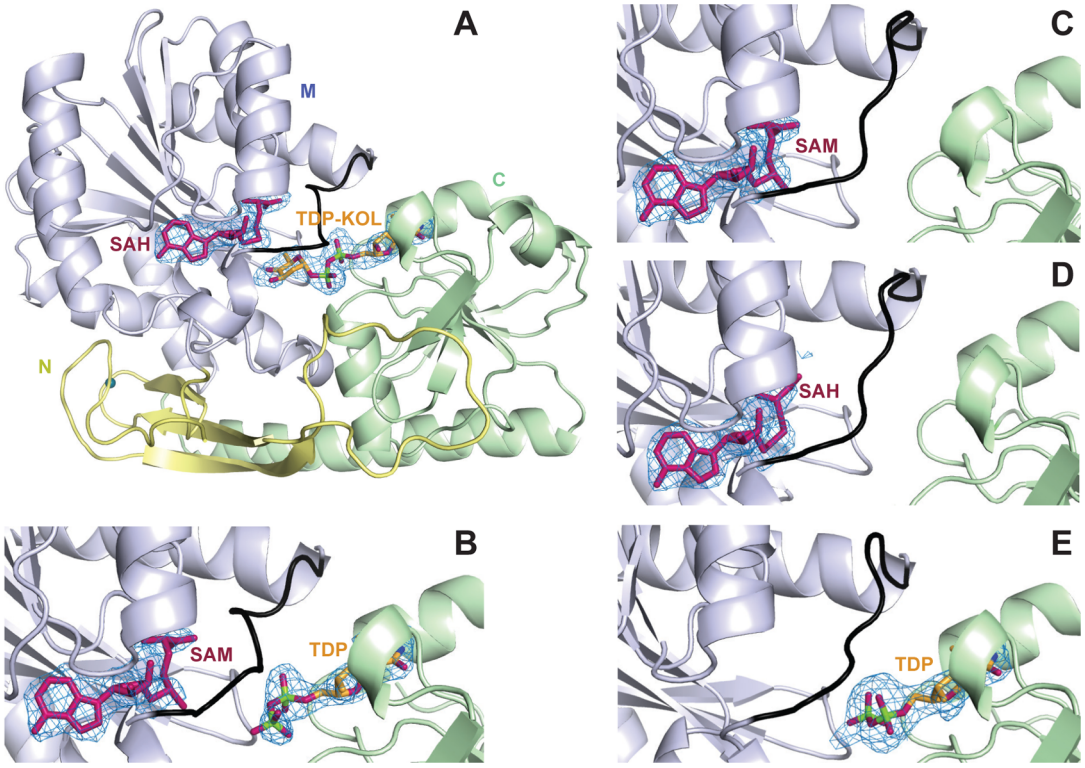

Figure 3. Cartoon representation of crystal structures of MtmC with its biologically relevant ligands. The N-terminal, central, and C-terminal domains are colored yellow, blue, and green, respectively. The ligands are shown as sticks; SAM and SAH are colored pink and the substrate and TDP orange. The sensor loop (residues 76−84) is colored black. The Zn^{2+} ion is shown as a red sphere. (A) Structure of MtmC-SAH-TDP-4-keto-olivose (MtmC-SAH-TDP-KOL). The close-up views of the active sites of MtmC-SAM-TDP, MtmC-SAM, MtmC-SAH, and MtmC-TDP complexes are shown in panels B−E, respectively.

SAH was measured. The rate of conversion of SAM to SAH for the wild-type enzyme and the two mutants was calculated from the 60 and 300 min data points.

RESULTS

Homologues of MtmC. A BLAST search[23] for MtmC homologues yielded a number of mostly putative bacterial class I family SAM-dependent sugar *C*-methyltransferases dominated by those from *Streptomyces*. MtmC homologues whose function has been demonstrated or postulated are listed in Table 2 together with the respective sugar moiety and the final natural product, whose biosynthesis they are involved in. The multiple-sequence alignment of MtmC and these homologues is given in Figure 1 of the Supporting Information. The only homologue of MtmC that has been rigorously characterized both functionally and structurally, by Holden and co-workers, is *C*-3′-methyltransferase TcaB9 from *Micromonospora chalcea*, from the biosynthetic pathway for D-tetronitrose in tetrocarcin A.[20,24] Structural information about MtmC would not only help elucidate its intriguing catalytic mechanism but also reveal divergent structural features of this family of *C*-methyltransferases responsible for recognition of specific sugar substrates.

Overview of Crystal Structures of MtmC with Its Substrates and Cosubstrates. We determined crystal

DOI: 10.1021/bi501462g
Biochemistry 2015, 54, 2481−2489

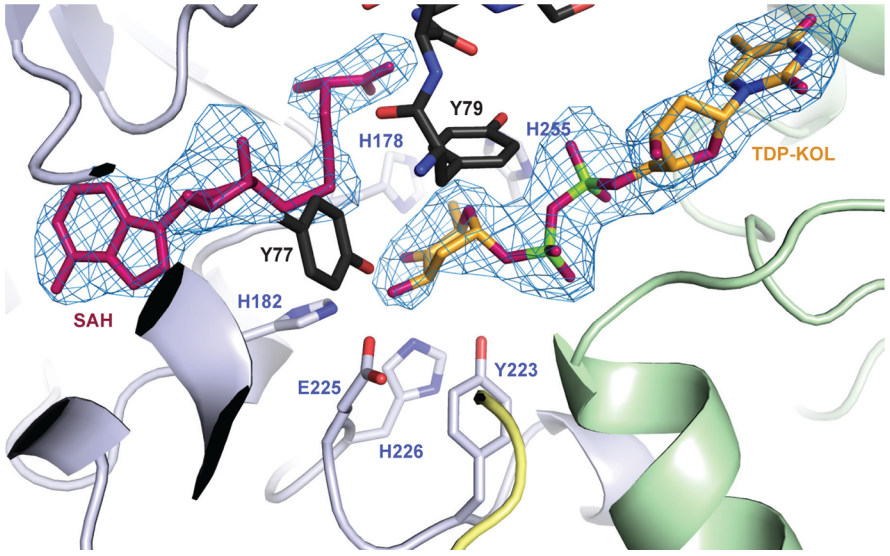

Figure 4. Active site of the MtmC-SAH-TDP-KOL complex. The ligands and the residues interacting with the sugar moiety of the substrate are shown as sticks and colored according to the protein region to which they belong, as in Figure 1.

structures of three binary complexes (MtmC-SAM, MtmC-SAH, and MtmC-TDP) and two ternary complexes (MtmC-SAH-TDP-4-keto-D-olivose and MtmC-SAH-TDP) (Figure 3). In all the structures, the ligands were very clearly resolved in the strong omit $F_o - F_c$ electron density map (Figure 3). The apo-MtmC did not form crystals suitable for a diffraction experiment, likely because of the mobility of protein regions involved in substrate or cosubstrate binding. The overall structure of MtmC is similar to that of TcaB9.[24] MtmC is a monomer with a tripartite fold. Its N-terminal domain (residues 1−68) consists of a β-sheet and extensive regions lacking secondary structure. As in TcaB9, these loop regions contain a tightly bound Zn^{2+} ion coordinated tetrahedrally to four conserved cysteines [Cys13, Cys16, Cys56, and Cys59 (Figure 3 and Figure 1 of the Supporting Information)]. The central domain (residues 69−288) and the C-terminal domain (residues 289−423) are structurally similar, with a Rossman-type fold forming a SAM and a TDP binding site, respectively. Except for one region of the central domain, whose residues interact with both SAM/SAH and the sugar moiety of the TDP-sugar substrate (residues 76−84; described in detail in the next section), all structures of MtmC are similar to each other.

MtmC-SAM and MtmC-SAH Complexes. In the crystal structures of MtmC-SAM and MtmC-SAH complexes, the cofactor and its product are bound in the conserved binding pocket formed by residues of the central domain, like the bound SAH in the crystal structure of TcAB9[24] (Figure 3A−D). The protein conformations in the complexes with SAM and SAH are nearly identical (Figure 3C,D). A striking difference in the substrate binding pocket between MtmC-SAM/SAH and TcaB9 structures is in the conformation of a loop region between residues 76 and 84, which we will call the sensor loop (Figure 3). The backbone of the sensor loop in MtmC switches its conformation based on whether the susbstrate or the cosubstrate occupies their respective binding pockets. In contrast, the conformation of this region in TcaB9 does not differ significantly among any of its binary and ternary complexes with the cosubstrate, substrate, or their products.[20,24] The conformations of the sensor loop of MtmC when only SAM/SAH or only TDP is bound allow relatively facile access to the active site from outside. In contrast, when both SAM and TDP are bound, this loop adopts a conformation that is more closed onto the active site. Finally, when both SAH and TDP-4′-keto-olivose are bound, the sensor loop fits in the most closed state, sterically blocking the dissociation of the ligands from it.

MtmC-SAH-TDP-4-keto-D-olivose, MtmC-SAM-TDP, and MtmC-TDP Structures. The ternary complex MtmC-SAH-TDP-4-keto-D-olivose represents a mimic of the reaction intermediate prior to the catalytic methyl transfer. Here, we observe a number of interactions that stabilize the bound substrate TDP-4-keto-D-olivose (Figure 4). These interactions are similar to those observed in the ternary complex TcaB9-SAH-TDP-3-amino-2,3,6-trideoxy-4-keto-D-glucose, except His178 of MtmC is replaced by Asn177 in TcaB9, both making a van der Waals contact between their respective C_β-methylene group and the 5-methyl group of the sugar. The environment of the 3-OH group of the sugar is highly hydrophilic, with the side chains of Glu225 and His182 engaged in hydrogen bonds with this hydroxyl group. Tyr77 is in the sensor loop; however, its conformation does not change significantly in different complexes, and its hydroxyl group appears to form a weak hydrogen bond with the 3-OH of the sugar (with an O−O distance of 3.35 Å). His226 forms a hydrogen bond with the 4-keto group of the olivose, consistent with its potential role as the catalytic acid, demonstrated for its counterpart in TcaB9, His225.[20] The 3-OH group of the sugar points toward the sulfur atom of SAH, indicating that the methylation occurs with inversion of stereochemistry at this position, in agreement with the biosynthetic pathway and the enzymatic properties of MtmC.[17] In contrast, the counterpart 3-amino group of TDP-3-amino-2,3,6-trideoxy-4-keto-D-glucose points away from the SAH in the complex with TcaB9, indicating that methylation by this enzyme occurs without inversion at this stereocenter.[24]

The sensor loop and especially Tyr79 exhibit a progression of conformational states in complexes MtmC-SAM/SAH, MtmC-TDP, MtmC-SAM-TDP, and MtmC-SAH-TDP-4-keto-D-olivose, as follows. In the MtmC-SAM and MtmC-SAH complexes (Figure 5A; MtmC-SAH is nearly identical),

DOI: 10.1021/bi501462g
Biochemistry 2015, 54, 2481−2489

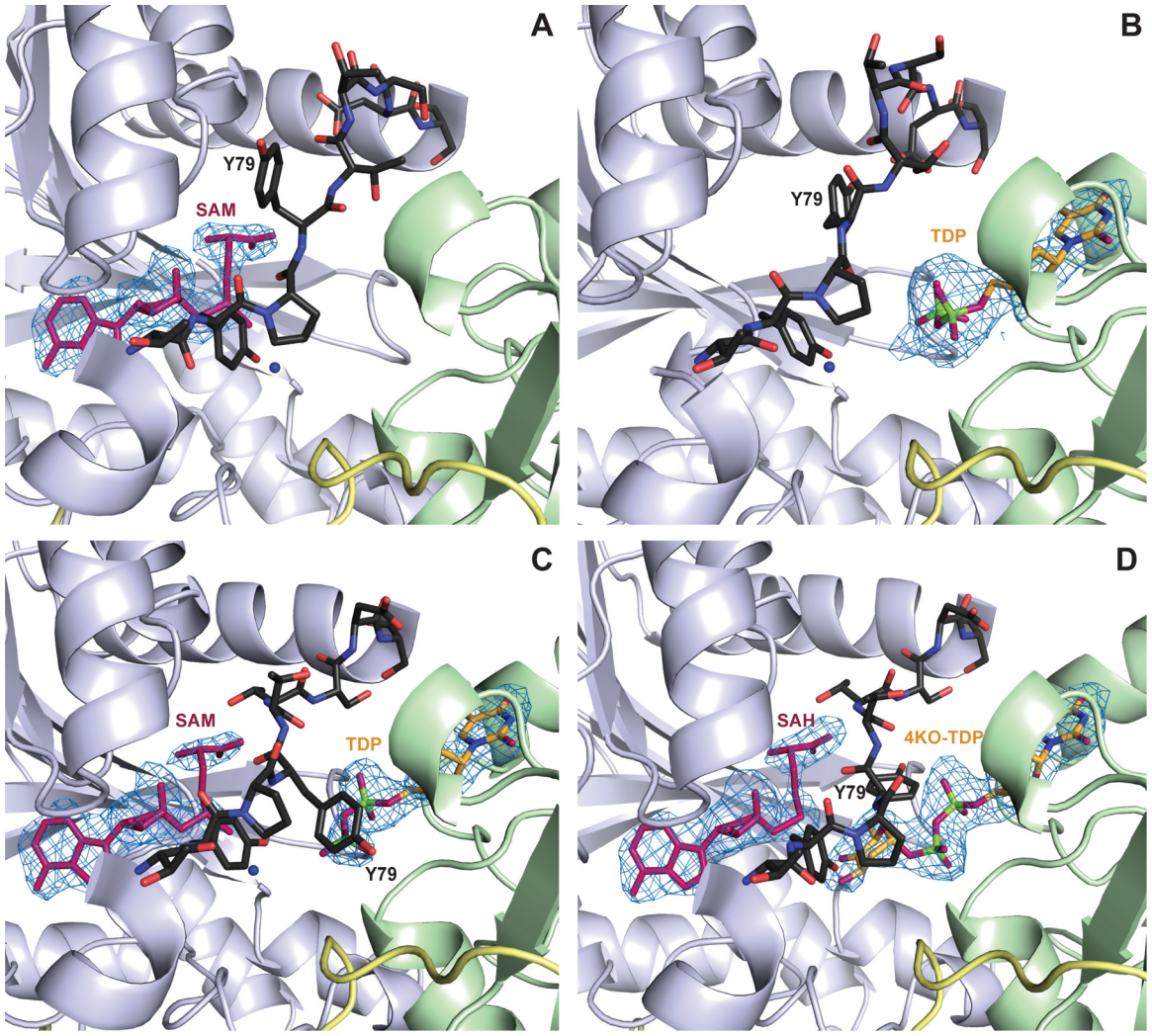

Figure 5. Different conformations of the sensor loop (black sticks) in (A) MtmC-SAM, (B) MtmC-TDP, (C) MtmC-SAM-TDP, and (D) MtmC-SAH-TDP-KOL complexes. The water molecule that occupies the site of the 3-OH group of the sugar in its absence is shown as a blue sphere.

Tyr79 points out of the active site. When only TDP is bound (Figure 5B), the sensor loop remains essentially unchanged, except for Tyr79, whose side chain is rotated by 130° where it does not interact with the TDP phosphates (Figure 5B). In the MtmC-TDP complex, the only complex not containing SAM or SAH, the sensor loop exhibits partial disorder, whereas it is well-ordered in the MtmC-SAM and MtmC-SAH complexes, indicating that this loop undergoes an order−disorder transition upon dissociation of SAH. This is consistent with Tyr77, Tyr79, and Thr81 in this loop forming a part of the cofactor binding interface in the ternary complexes (Figures 4 and 5C,D). In the ternary complex MtmC-SAM-TDP (Figure 5C), the backbone of the sensor loop around Tyr79 is moved toward the active site, with Tyr79 pointing out of the active center. In this conformation, Tyr79 does not interact with either SAM or TDP, apparently because the previous conformation would place the aromatic ring of Tyr79 in the unfavorable charged environment of the TDP phosphate groups. In all the complexes mentioned above, waters fill empty cosubstrate or substrate binding pockets. Specifically, in complexes MtmC-SAM/SAH and MtmC-TDP, a water molecule is invariably found in place of the 3-OH group of the sugar (Figure 5A−C). In complex MtmC-SAH-TDP-4-keto-D-olivose (Figure 5D), the sensor loop stays in the same backbone conformation, and Tyr79 is in a different rotamer state (different from that in the MtmC-SAM complex by 180°), capping the substrate by the steric contact between the phenol ring of Tyr79 and the nonpolar sugar-β-phosphate junction as well as making a hydrogen bond between the hydroxyl group of Tyr79 and the α-phosphate. In addition, in this conformation, Tyr79 interacts sterically with SAH. This conformation of the sensor loop and Tyr79 is similar to that observed in all structures of TcaB9, with and without the substrates, cosubstrates, or products. Therefore, unlike TcaB9, MtmC exhibits conformational plasticity of the sensor loop and its residues, especially Tyr79.

Methyltransferase Activity of MtmC Mutants Tyr79-Ala and Tyr79Phe. To probe the functional importance of Tyr79, we measured the rate of SAH formation upon methyl transfer. We found that Tyr79Ala and Tyr79Phe mutants of MtmC catalyzed the methyl transfer ~7−8 times less efficiently than wild-type MtmC did (Figure 6). This demonstrated the functional importance of the hydroxyl group of the Tyr79 in positioning the substrate for catalysis, consistent with its interaction with the α-phosphate of the TDP moiety shown by the structural analysis.

DOI: 10.1021/bi501462g
Biochemistry 2015, 54, 2481−2489

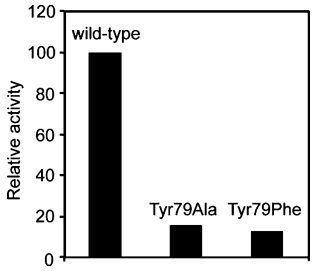

Figure 6. Effect of mutations of Tyr79 on the methyltransferase activity of MtmC. Shown are methyltransferase activities of wild-type MtmC and its mutants, Tyr79Phe and Tyr79Ala, relative to that of the wild-type enzyme.

DISCUSSION

An intriguing enzyme complex MtmC/MtmGIV plays a key role in the biosynthesis of the important trisaccharide chain of the anticancer drug mithramycin. As a stepping stone toward elucidation of how these two enzymes cooperate, we determine the protein crystal structure of ketoreductase/*C*-methyltransferase MtmC. We obtained crystal structures of MtmC with its biologically relevant ligands, including that of the ternary complex of MtmC with bound substrate 4-keto-D-olivose and SAH. Because the TDP-sugar binding pocket appears to be highly conserved in this family of methyltransferases, and the only other access to the sugar moiety (without a major protein conformational change) is via the SAM binding channel, MtmC must use the same channel to bind either NADPH or SAM, depending on the catalytic function. The conformationally versatile sensor loop and, specifically, Tyr79 likely play an important role in active site dehydration and the control of substrate and cosubstrate binding and product release. Our biochemical and structural data explain the universal conservation of this Tyr among MtmC and its homologues (Figure 1 of the Supporting Information): the hydrogen bond between the OH of Tyr79 and the TDP moiety is important for the catalytic turnover, because the Tyr79Phe mutant is catalytically compromised. Moreover, Tyr79 is likely needed to ensure discrimination of the sugar-TDP from TDP or other abundant ligands, via its ability to establish a bidentate interaction with both the sugar and the TDP moieties of the substrate, while also making a contact with SAM. Indeed, Tyr79 is seen in the conformation ensuring such interaction only in the ternary complex MtmC-SAH-TDP-4-keto-D-olivose, but not in complex MtmC-SAM-TDP. Because the active site pocket appears to be too constricted for binding of the larger cofactor, NADPH, when Tyr79 is in the "in" conformation, we propose that MtmC has uniquely evolved to accommodate NADPH by swinging Tyr79 out of the active site to make room for NADPH binding. In support of this idea, the TcaB9, which is a monofunctional methyltransferase, the homologous Tyr78 does not appear to undergo this conformational change. We modeled NADPH bound to MtmC in this Tyr79 "out" conformation (Figure 7); the nicotinic acid moiety of NADPH in this model is in place of the phenol ring of Tyr79 in the "in" conformation, with the ribose rings of SAM and SAH occupying the same site. Because NADPH is larger than SAM, the adenine base of NADPH in the model is more solvent-exposed, as expected, because the binding site has evolved to bind mainly SAM in this family of enzymes. Indeed, as we observed only partial density for NADPH in the crystals grown or soaked with NADPH or NADPH and the substrate (insufficient for building its structure in the active site of MtmC), NADPH is likely only loosely bound.

The structures of MtmC and TcaB9 in complexes with their respective substrates together with the sequence alignment (Table 2 and Figure 1 of the Supporting Information) allow one to analyze potential sugar recognition and regiospecificity rules among close homologues of MtmC. Interestingly, some of the homologues function as 5-methyltransferases, methylating a position symmetrical with respect to a 180° rotation around the axis going through positions 1−4 of the sugar ring. Such rotation is needed to expose position 5 for methylation, and consequently, the ring oxygen of the sugar will then be located in place of the 2-methylene group in the structure of MtmC-

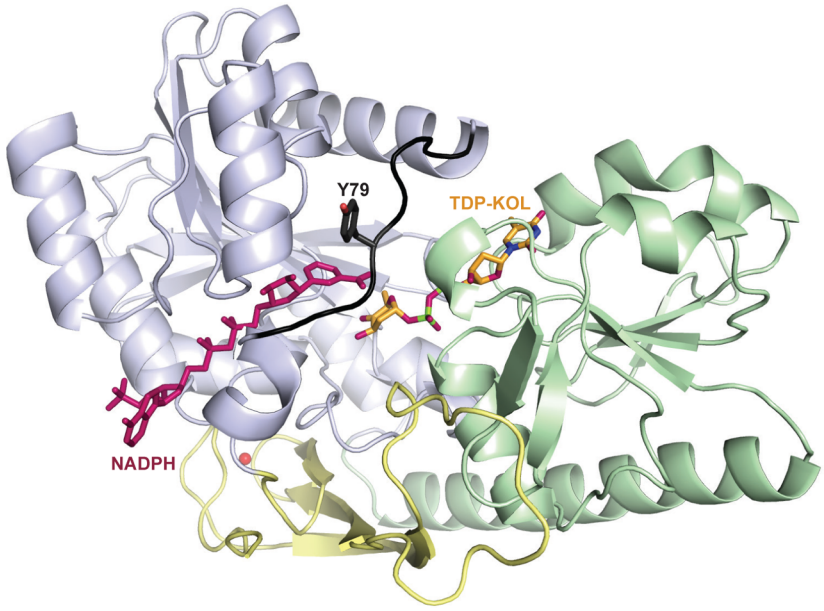

Figure 7. Model of the MtmC-NADPH-TDP-KOL complex. In this model, the conformation of MtmC from the structure of MtmC-SAM (Figure 5A) was used.

DOI: 10.1021/bi501462g
Biochemistry 2015, 54, 2481−2489

SAH-TDP-KOL. These 5-*C*-methyltransferases are CloU,[25] CouU,[26,27] and NovU[28] from the clorobiocin, coumermycin A_1, and novobiocin biosynthetic pathways, respectively, and a more divergent homologue TiaS2[29] from the tiacumicin B pathway. The 2-methylenes in the MtmC and TcaB9 structures in complexes with their respective substrates are dehydrated and are not close to potential hydrogen bond donors. The side chain of Asp34 that points toward this sugar position is too distant to interact with it, and instead, Asp34 interacts with a potential catalytic residue Glu225. Interestingly, in CloU, CouU, and NovU, Asp34 is replaced by a Gly, creating a void. A coupled residue difference in these three 5-*C*-methyltransferases is a replacement of Pro78 in the sensor loop by an Arg. These two changes may either expose this position, now occupied by a ring oxygen, to solvent or, through a potential conformational change of the backbone due to the Pro78 substitution, provide the Arg as a hydrogen bond donor for the ring oxygen. TiaS2 appears to be a special case, where Asp34 is not replaced and Pro78 is replaced by a Val. However, TiaS2 is also the only exception in that in place of Tyr223 it contains a His, which has a potential for formation of strong hydrogen bonds. In even more divergent 3-*C*-methyltransferases EryBIII,[30] TylCIII,[31] and AviG1,[32] a Gly is in place of both Asp34 and Pro78, but a Cys in place of Tyr223 may preserve the overall dehydrated environment of the methylene at position 2. These last three examples are more speculative, because the sensor loop sequence in these homologues is very different from that of MtmC and is very Gly- and Ser-rich; therefore, its conformation may not be well predicted by the structures of MtmC and TcaB9. Finally, a much smaller Cys in place of Tyr223 in EryBIII is able to accommodate a bulky methoxy group that is also installed at position 3, which would otherwise clash with a Tyr.

While both the sugar donor substrate generation and transfer are catalyzed by MtmC, MtmTIII, and MtmGIV for the first and the third sugar of the trisaccharide chain, the overall biosynthetic sequence of the trisaccharide chain biosynthesis necessitates one MtmC-independent step between them, namely the transfer of D-oliose, the second sugar of the chain, by MtmGIII. Thus, many intriguing questions remain. For example, how is the product of the first MtmC/MtmGIV reaction passed onto MtmGIII and then back to MtmC/MtmGIV? Are all three enzymes somehow assembled into a multienzyme complex? We hope that complementary ongoing structural studies of MtmGIV and MtmTIII will shed light on these questions.

■ ASSOCIATED CONTENT

Supporting Information

Supplementary Figure 1. This material is available free of charge via the Internet at http://pubs.acs.org.

■ AUTHOR INFORMATION

Corresponding Authors

*Department of Pharmaceutical Sciences, College of Pharmacy, University of Kentucky, 789 S. Limestone St., Lexington, KY 40536-0596. E-mail: jrohr2@email.uky.edu. Phone: (859) 323-5031. Fax: (859) 257-7564.

*E-mail: ovts222@uky.edu. Phone: (859) 218-1687. Fax: (859) 257-7585.

Funding

This work was supported by grants from the National Institutes of Health (CA 091901 and GM 105977) to J.R. and start-up funds from University of Kentucky College of Pharmacy to O.V.T.

Notes

The authors declare no competing financial interest.

■ ACKNOWLEDGMENTS

We thank the staff of sectors 21 and 22 of the Advanced Photon Source at the Argonne National Laboratory for assistance with X-ray diffraction data collection.

■ ABBREVIATIONS

MTM, mithramycin; MT, methyltransferase; PCR, polymerase chain reaction; HPLC, high-performance liquid chromatography; DMSO, dimethyl sulfoxide; LB, Lysogeny broth; IPTG, isopropyl β-D-1-thiogalactopyranoside; IMAC, immobilized metal ion affinity chromatography; Tris, tris(hydroxymethyl)-aminomethane; TBE, Tris/borate/EDTA; MS, mass spectrometry; HRMS, high-resolution mass spectrometry; NMR, nuclear magnetic resonance; ESI-MS, electrospray ionization mass spectrometry; HRESI-MS, high-resolution electrospray ionization mass spectrometry; TDP, thymidine diphosphate; TDP-KOL, TDP-4-keto-D-olivose; SAM, *S*-adenosylmethionine; SAH, *S*-adenosylhomocysteine; NADPH, nicotinamide adenine dinucleotide phosphate; GDD, 5,5-*gem*-dimethyl deoxysugar.

■ REFERENCES

(1) Skarbek, J. D., and Speedie, M. K. (1981) Antitumor antibiotics of the aureolic acid group: Chromomycin A3, mithramycin A, and olivomycin A. In *Antitumor compounds of natural origin: Chemistry and biochemistry* (Aszalos, A., Ed.) pp 191−235, CRC Press, Boca Raton, FL.

(2) Lombó, F., Menendez, N., Salas, J. A., and Méndez, C. (2006) The aureolic acid family of antitumor compounds: Structure, mode of action, biosynthesis, and novel derivatives. *Appl. Microbiol. Biotechnol. 73*, 1−14.

(3) Katahira, R., Uosaki, Y., Ogawa, H., Yamashita, Y., Nakano, H., and Yoshida, M. (1998) UCH9, a new antitumor antibiotic produced by *Streptomyces*. II. Structure elucidation of UCH9 by mass and NMR spectroscopy. *J. Antibiot. 51*, 267−274.

(4) Jayasuriya, H., Lingham, R. B., Graham, P., Quamina, D., Herranz, L., Genilloud, O., Gagliardi, M., Danzeisen, R., Tomassini, J. E., Zink, D. L., Guan, Z. Q., and Singh, S. B. (2002) Durhamycin A, a potent inhibitor of HIV Tat transactivation. *J. Nat. Prod. 65*, 1091−1095.

(5) Majee, S., Sen, R., Guha, S., Bhattacharyya, D., and Dasgupta, D. (1997) Differential Interactions of the Mg^{2+} Complexes of chromomycin A_3 and mithramycin with poly(dG-dC)·poly(dC-dG) and poly(dG)·poly(dC). *Biochemistry 36*, 2291−2299.

(6) Silva, D. J., Goodnow, R., Jr., and Kahne, D. (1993) The sugars in chromomycin A3 stabilize the Mg^{2+}-dimer complex. *Biochemistry 32*, 463−471.

(7) Bianchi, N., Osti, F., Rutigliano, C., Corradini, F. G., Borsetti, E., Tomassetti, M., Mischiati, C., Feriotto, G., and Gambari, R. (1999) The DNA-binding drugs mithramycin and chromomycin are powerful inducers of erythroid differentiation of human K562 cells. *Br. J. Haematol. 104*, 258−265.

(8) Grohar, P. J., Woldemichael, G. M., Griffin, L. B., Mendoza, A., Chen, Q. R., Yeung, C., Currier, D. G., Davis, S., Khanna, C., Khan, J., McMahon, J. B., and Helman, L. J. (2011) Identification of an inhibitor of the EWS-FLI1 oncogenic transcription factor by high-throughput screening. *J. Natl. Cancer Inst. 103*, 962−978.

(9) Zhang, M., Mathur, A., Zhang, Y., Xi, S., Atay, S., Hong, J. A., Datrice, N., Upham, T., Kemp, C. D., Ripley, R. T., Wiegand, G.,

DOI: 10.1021/bi501462g
Biochemistry 2015, 54, 2481−2489

Avital, I., Fetsch, P., Mani, H., Zlott, D., Robey, R., Bates, S. E., Li, X., Rao, M., and Schrump, D. S. (2012) Mithramycin represses basal and cigarette smoke-induced expression of ABCG2 and inhibits stem cell signaling in lung and esophageal cancer cells. *Cancer Res. 72*, 4178−4192.
(10) Menéndez, N., Nur-e-Alam, M., Braña, A. F., Rohr, J., Salas, J. A., and Méndez, C. (2004) Tailoring modification of deoxysugars during biosynthesis of the antitumour drug chromomycin A by *Streptomyces griseus* ssp. *griseus*. *Mol. Microbiol. 53*, 903−915.
(11) Menéndez, N., Nur-e-Alam, M., Braña, A. F., Rohr, J., Salas, J. A., and Méndez, C. (2004) Biosynthesis of the antitumor chromomycin A3 in *Streptomyces griseus*: Analysis of the gene cluster and rational design of novel chromomycin analogs. *Chem. Biol. 11*, 21−32.
(12) Menéndez, N., Nur-e-Alam, M., Fischer, C., Braña, A. F., Salas, J. A., Rohr, J., and Méndez, C. (2006) Deoxysugar transfer during chromomycin A3 biosynthesis in *Streptomyces griseus* subsp. *griseus*: New derivatives with antitumor activity. *Appl. Environ. Microbiol. 72*, 167−177.
(13) Montanari, A., and Rosazza, J. P. (1990) Biogenesis of chromomycin A3 by *Streptomyces griseus*. *J. Antibiot. 43*, 883−889.
(14) Remsing, L. L., Garcia-Bernardo, J., Gonzalez, A. M., Künzel, E., Rix, U., Braña, A. F., Bearden, D. W., Méndez, C., Salas, J. A., and Rohr, J. (2002) Ketopremithramycins and ketomithramycins, four new aureolic acid-type compounds obtained upon inactivation of two genes involved in the biosynthesis of the deoxysugar moieties of the antitumor drug mithramycin by *Streptomyces argillaceus*, reveal novel insights into post-PKS tailoring steps of the mithramycin biosynthetic pathway. *J. Am. Chem. Soc. 124*, 1606−1614.
(15) Gonzalez, A., Remsing, L. L., Lombó, F., Fernandez, M. J., Prado, L., Braña, A. F., Künzel, E., Rohr, J., Méndez, C., and Salas, J. A. (2001) The mtmVUC genes of the mithramycin gene cluster in *Streptomyces argillaceus* are involved in the biosynthesis of the sugar moieties. *Mol. Gen. Genet. 264*, 827−835.
(16) Nur-e-Alam, M., Méndez, C., Salas, J. A., and Rohr, J. (2005) Elucidation of the glycosylation sequence of mithramycin biosynthesis: Isolation of 3A-deolivosylpremithramycin B and its conversion to premithramycin B by glycosyltransferase MtmGII. *ChemBioChem 6*, 632−636.
(17) Wang, G., Pahari, P., Kharel, M. K., Chen, J., Zhu, H., Van Lanen, S. G., and Rohr, J. (2012) Cooperation of two bifunctional enzymes in the biosynthesis and attachment of deoxysugars of the antitumor antibiotic mithramycin. *Angew. Chem., Int. Ed. 51*, 10638−10642.
(18) Otwinowski, Z., and Minor, W. (1997) Processing of X-ray diffraction data collected in oscillation mode. *Methods Enzymol. 276*, 307−326.
(19) Vagin, A., and Teplyakov, A. (2010) Molecular replacement with MOLREP. *Acta Crystallogr. D66*, 22−25.
(20) Bruender, N. A., Thoden, J. B., Kaur, M., Avey, M. K., and Holden, H. M. (2010) Molecular architecture of a C-3′-methyltransferase involved in the biosynthesis of D-tetronitrose. *Biochemistry 49*, 5891−5898.
(21) Emsley, P., and Cowtan, K. (2004) Coot: Model-building tools for molecular graphics. *Acta Crystallogr. D60*, 2126−2132.
(22) Murshudov, G. N., Vagin, A. A., and Dodson, E. J. (1997) Refinement of macromolecular structures by the maximum-likelihood method. *Acta Crystallogr. D53*, 240−255.
(23) Altschul, S. F., Gish, W., Miller, W., Myers, E. W., and Lipman, D. J. (1990) Basic local alignment search tool. *J. Mol. Biol. 215*, 403−410.
(24) Bruender, N. A., and Holden, H. M. (2012) Probing the catalytic mechanism of a C-3′-methyltransferase involved in the biosynthesis of D-tetronitrose. *Protein Sci. 21*, 876−886.
(25) Freitag, A., Li, S. M., and Heide, L. (2006) Biosynthesis of the unusual 5,5-gem-dimethyl-deoxysugar noviose: Investigation of the C-methyltransferase gene *cloU*. *Microbiology 152*, 2433−2442.
(26) Wang, Z. X., Li, S. M., and Heide, L. (2000) Identification of the coumermycin A(1) biosynthetic gene cluster of *Streptomyces rishiriensis* DSM 40489. *Antimicrob. Agents Chemother. 44*, 3040−3048.
(27) Li, S. M., Westrich, L., Schmidt, J., Kuhnt, C., and Heide, L. (2002) Methyltransferase genes in *Streptomyces rishiriensis*: New coumermycin derivatives from gene-inactivation experiments. *Microbiology 148*, 3317−3326.
(28) Thuy, T. T., Lee, H. C., Kim, C. G., Heide, L., and Sohng, J. K. (2005) Functional characterizations of *novWUS* involved in novobiocin biosynthesis from *Streptomyces spheroides*. *Arch. Biochem. Biophys. 436*, 161−167.
(29) Xiao, Y., Li, S., Niu, S., Ma, L., Zhang, G., Zhang, H., Ju, J., and Zhang, C. (2011) Characterization of tiacumicin B biosynthetic gene cluster affording diversified tiacumicin analogues and revealing a tailoring dihalogenase. *J. Am. Chem. Soc. 133*, 1092−1105.
(30) Gaisser, S., Bohm, G. A., Doumith, M., Raynal, M. C., Dhillon, N., Cortes, J., and Leadlay, P. F. (1998) Analysis of *eryBI*, *eryBIII* and *eryBVII* from the erythromycin biosynthetic gene cluster in *Saccharopolyspora erythraea*. *Mol. Gen. Genet. 258*, 78−88.
(31) Takahashi, H., Liu, Y. N., Chen, H., and Liu, H. W. (2005) Biosynthesis of TDP-l-mycarose: The specificity of a single enzyme governs the outcome of the pathway. *J. Am. Chem. Soc. 127*, 9340−9341.
(32) Weitnauer, G., Gaisser, S., Kellenberger, L., Leadlay, P. F., and Bechthold, A. (2002) Analysis of a C-methyltransferase gene (aviG1) involved in avilamycin biosynthesis in *Streptomyces viridochromogenes* Tu57 and complementation of a *Saccharopolyspora erythraea eryBIII* mutant by *aviG1*. *Microbiology 148*, 373−379.
(33) Laskowski, R. A., Macarthur, M. W., Moss, D. S., and Thornton, J. M. (1993) Procheck: A program to check the stereochemical quality of protein structures. *J. Appl. Crystallogr. 26*, 283−291.
(34) Torkkell, S., Kunnari, T., Palmu, K., Mantsala, P., Hakala, J., and Ylihonko, K. (2001) The entire nogalamycin biosynthetic gene cluster of *Streptomyces nogalater*: Characterization of a 20-kb DNA region and generation of hybrid structures. *Mol. Genet. Genomics 266*, 276−288.
(35) Chen, H., Thomas, M. G., Hubbard, B. K., Losey, H. C., Walsh, C. T., and Burkart, M. D. (2000) Deoxysugars in glycopeptide antibiotics: Enzymatic synthesis of TDP-L-epivancosamine in chloroeremomycin biosynthesis. *Proc. Natl. Acad. Sci. U.S.A. 97*, 11942−11947.

DOI: 10.1021/bi501462g
Biochemistry 2015, 54, 2481−2489